

Full paper / Mémoire

Physical mechanisms of bacterial survival revealed by combined grazing-incidence X-ray scattering and Monte Carlo simulation

Rafael G. Oliveira ^{a,1}, Emanuel Schneck ^{a,b}, Bonnie E. Quinn ^{c,d}, Oleg V. Konovalov ^e,
Klaus Brandenburg ^f, Ulrich Seydel ^f, Tom Gill ^{d,g}, Charles B. Hanna ^{d,h},
David A. Pink ^{c,d,*}, Motomu Tanaka ^{a,b,d,**}

^a Biophysics Laboratory E22, Technical University Munich, D85748 Garching, Germany

^b Biophysical Chemistry Laboratory II, Institute of Physical Chemistry and BIOQUANT, University of Heidelberg, D69120 Heidelberg, Germany

^c Department of Physics, St. Francis Xavier University, Antigonish, NS B2G 2W5, Canada

^d Advanced Foods and Materials Network of Centres of Excellence, Canada

^e European Synchrotron Radiation Facility (ESRF), 38053 Grenoble, Cedex 9, France

^f Research Center Borstel, D23845 Borstel, Germany

^g Institute of Fisheries Technology, Dalhousie University, Halifax, NS B3J 2X4, Canada

^h Department of Physics, Boise State University, Boise, ID 83725-1570, USA

Received 14 March 2008; accepted after revision 18 June 2008

Available online 17 November 2008

Abstract

The combination of grazing-incidence X-ray scattering experiments and Monte Carlo simulation unravels the physics of bacterial survival against cationic antimicrobial peptides (protamine). As a realistic model of bacterial outer membranes, an insoluble monolayer of lipopolysaccharide from *Salmonella enterica* sv. Minnesota Ra (LPS Ra) is spread on buffered subphase. In the presence of Ca²⁺, vertical electron density profiles reconstructed from X-ray scattering imply the “collapse” of saccharide chains, suggesting that Ca²⁺ bridges the negatively charged saccharide units. Under this condition, the LPS monolayer remains intact even after injection of protamine near the minimum inhibitory concentration. This can theoretically be accounted in terms of the formation of an electrostatic energy barrier that prevents the approach of protamine to the hydrophobic region. In contrast, as predicted from in vivo experiments, the intrusion of protamine in the absence of Ca²⁺ results in the complete destruction of the layered structure of LPS Ra monolayers. **To cite this article:** Rafael G. Oliveira et al., *C. R. Chimie* 12 (2009).

© 2008 Académie des sciences. Published by Elsevier Masson SAS. All rights reserved.

Résumé

La combinaison de la diffraction des rayons X en incidence rasante et des simulations Monte Carlo permet de dévoiler la physique de la survie bactérienne en présence de peptides antimicrobiens cationiques (protamine). Un modèle réaliste de la membrane externe des bactéries, une monocouche insoluble de lipo-polysaccharides de *Salmonella enterica* sv. Minnesota Ra (LPS

* Corresponding author. Department of Physics, St. Francis Xavier University, Antigonish, NS, B2G 2W5, Canada.

** Corresponding author. Biophysical Chemistry Laboratory II, Institute of Physical Chemistry and BIOQUANT, University of Heidelberg, D69120 Heidelberg, Germany.

E-mail addresses: scorpiocarla@gmail.com (D.A. Pink), tanaka@uni-heidelberg.de (M. Tanaka).

¹ Present address: CIQUIBIC-UNC, Ciudad Universitaria X5000HUA, Córdoba, Argentina.

Ra), est étalée à la surface d'une solution aqueuse. En présence d'ions Ca^{2+} , les profils de densité électronique, reconstruits par diffraction des rayons X, montrent l'effondrement des chaînes de saccharide et suggèrent que les ions Ca^{2+} pontent les unités de saccharide chargées négativement. Dans ces conditions, la monocouche de LPS reste intacte même après injection de protamine à une concentration proche de la concentration critique d'inhibition. En revanche, comme cela est prédit par des expériences in vivo, l'intrusion de protamine en l'absence de Ca^{2+} entraîne la destruction complète de la structure stratifiée des monocouches de LPS Ra. **Pour citer cet article :** Rafael G. Oliveira et al., C. R. Chimie 12 (2009).

© 2008 Académie des sciences. Published by Elsevier Masson SAS. All rights reserved.

Keywords: Lipopolysaccharide; Antibacterial peptide; Monolayer; Grazing-incidence X-ray scattering; Monte Carlo simulation

Mots-clés : Lipo-polysaccharide ; Peptide antibactérien ; Monocouche ; Diffraction des rayons X en incidence rasante ; Simulation Monte Carlo

1. Introduction

Lipopolysaccharides (LPSs) are a major component of the outer leaflet of the outer membrane of Gram-negative bacteria, which stabilize the structural integrity of bacteria and protect the membrane against chemical attacks. LPSs are also known as endotoxins inducing a strong immune response because they bind to the receptor complex that promotes the secretion of pro-inflammatory cytokines. In recent years, cationic antimicrobial peptides (CAPs) have been drawing an increasing attention in food industry and medical sciences as antimicrobial alternatives to chemical food preservatives and commonly used antibiotics [1]. For example, protamine, a cationic peptide ($\text{pI} = 10\text{--}12$) extracted from the sperm cells of vertebrates, has been used as a food preservative in Japan. Many in vivo studies demonstrated that divalent cations (Ca^{2+} , Mg^{2+}) significantly increase the survival rate of bacteria, which suggests that electrostatic forces are responsible to let the positively charged protamine contact the negatively charged bacterial cell envelope [2–4].

To date, there have been several theoretical approaches to model the conformation of LPS molecules. Kotra et al. [5] used atomic-scale molecular dynamics to model a monolayer of 16 LPS molecules with 64 Mg^{2+} at $T = 300$ K, for a total simulation time of 200 ps. Straatsma and co-workers [6,7] constructed models of outer membranes of *Pseudomonas aeruginosa*, consisting of 16 LPS molecules in the outer and 40 phosphatidylethanolamine molecules in the inner leaflet, and ran isothermal–isobaric simulations for 1 ns, studying the distribution and dynamics of Ca^{2+} and saccharide moieties. These studies demonstrated that (i) divalent cations were essential for the stability of the LPS monolayer [5,7]; (ii) most of Ca^{2+} were confined to a “thin layer (2 nm) in the inner core” [6]; (iii) the location of the Ca^{2+} in the inner core region is well

defined with an average coordination number of Ca^{2+} to be 6.1, so that the mobility of negatively charged saccharides complexed with Ca^{2+} is lower than that of uncharged saccharides [6,7]; and (iv) water penetrated the membrane to a depth of ~ 30 Å [7]. More recently, Pink et al. [8] employed a “minimum model” of charged wild type LPS strains, conducted Monte Carlo (MC) simulations of the number-density distributions of ions and saccharides, then included protamine molecules in the model. They predict that the presence of divalent cations would replace protamines in the charged region, which results in a shift of the protamine distribution towards the aqueous solution. However, although this simulation qualitatively explains the increase of the minimum inhibitory concentration (MIC) very well, the structural evidence from experimental approaches at the molecular level is still missing.

This paper deals with a LPS purified from *Salmonella enterica* sv. Minnesota Ra, which is called as LPS Ra in the following. This LPS molecule consists of lipid A (with two phosphorylated *N*-acetylglucosamine units and six hydrocarbon chains) and the R polysaccharide unit (core). The latter comprises (a) the inner core of four negatively charged saccharide units: two 2-keto-3-deoxyoctonoic acid (KDO) units and two phosphorylated heptose units, and (b) the outer core of five uncharged saccharides [9]. Among LPS molecules from various rough (R) mutants, LPS Ra has the molecular structure which is closest to that of the bioactive fraction within the heterogeneous wild type LPS [10], possessing identical cores. This molecule lacks the *O*-polysaccharide (*O*-side chain), which is known to be highly poly-disperse. Here, LPS Ra molecules are spread on buffer subphase with and without Ca^{2+} , and form insoluble (Langmuir-type) monolayers at the air/water interface. Thus, LPS monolayers can be used as one of the simplest model systems that physically mimic the outermost surface of bacteria in contact with the surrounding environment, displaying well-defined

carbohydrate chains. This permits us to apply “slab” models that approximate the system as the stack of different slabs that possess defined electron density, thickness, and interface roughness.

To study the conformational change of carbohydrate chains due to Ca^{2+} , the electron density profiles normal to the surface are quantitatively reconstructed from grazing-incidence diffuse X-ray scattering out of the specular plane (GIXOS) [11]. GIXOS at the air/water interface offers a unique advantage over the specular reflectivity technique by significantly reducing the irradiation time (by a factor of 100), and thus minimizing the radiation damage to biological samples.

To study the impact of protamine on the film structures in the presence and absence of Ca^{2+} , we inject protamine from herring into the subphase while keeping the area of pre-formed monolayers constant (i.e. at a constant lateral density of LPS molecules). The interaction of protamine and LPS Ra is monitored by the change in surface pressure, as well as by the scattering signals. The use of LPS Ra also enables us to identify whether the electrostatic energy barrier created by the replacement of Na^+ by Ca^{2+} in the inner core region is sufficient for protection against protamine attack or whether the presence of an *O*-polysaccharide layer is essential.

To model the number-density profiles of different ion species, saccharide units, and protamine molecules, we created a “minimum model” using linearized Poisson–Boltzmann theory and carry out MC simulations. The average membrane plane (*xy*-plane) of our simulation volume possesses 100 LPS molecules, and the *z*-component of the simulation volume ranges from $0 \leq z \leq 200 \text{ \AA}$. Similar to the experimental resolution, we set the resolution of our theoretical slabs to be $\sim 2 \text{ \AA}$ in order to take thermal fluctuations of saccharide chains into account. Details on the experimental results and simulations are discussed in the following sections.

2. Results and discussion

2.1. Pressure–area isotherms

Fig. 1 represents the pressure–area isotherms of LPS Ra monolayers at the air/water interface on two types of subphases: (i) “ Ca^{2+} -free” buffer and (ii) “ Ca^{2+} -loaded” buffer (cf. Section 4). The absence of a plateau-like regime in both isotherms indicates that the hydrocarbon chains remain disordered (fluid). This can be confirmed by grazing-incidence X-ray diffraction (GIXD) experiments at wide angles [12,13], where no Bragg peak can be detected at all lateral pressures (data not shown). On Ca^{2+} -free buffer, the onset of

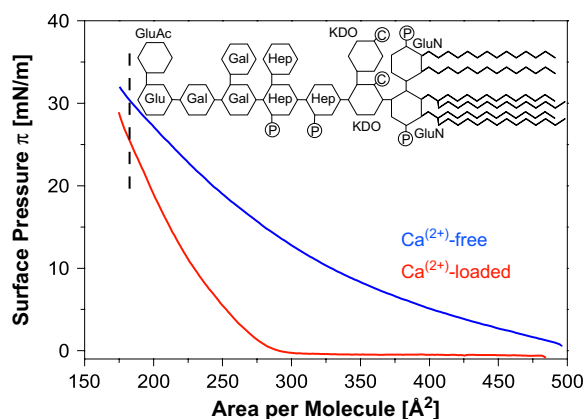


Fig. 1. Pressure–area isotherms of LPS Ra monolayers on Ca^{2+} -free (blue) and Ca^{2+} -loaded (red) buffers at 20°C . The schematic molecular structure of the LPS Ra is shown as an inset. The difference in the onset of the pressure increase and the calculated lateral compressibility of the monolayers suggest that the presence of Ca^{2+} makes the saccharide headgroups more compact, and thus increases the intermolecular cooperativity in LPS Ra monolayers. The vertical dashed line indicates the area per molecule of $A = 180 \text{ \AA}^2$ at which the GIXOS and protamine adsorption experiments are performed. *Abbreviations*. C: carboxylate, Gal: galactose, Glu: glucose, GluN: glucosamine, GluAc: *N*-acetylglucosamine, Hep: heptose, KDO: 2-keto-3-deoxyoctanate, P: phosphate.

pressure increase appears at $A > 500 \text{ \AA}^2$, corresponding to the interaction between neighboring saccharide headgroups. This is almost two times larger than that on Ca^{2+} -loaded buffer ($A \sim 280 \text{ \AA}^2$), suggesting that headgroups immersed in Ca^{2+} -free buffer occupy much larger areas than those in Ca^{2+} -loaded buffer. The lateral compressibilities calculated from the isotherms, $\chi = -(1/A)(\partial A/\partial \pi)$, are $\chi_{\text{free}} \sim 0.025 \text{ mN}^{-1} \text{ m}$ and $\chi_{\text{loaded}} \sim 0.013 \text{ mN}^{-1} \text{ m}$ at 180 \AA^2 , implying that the headgroups on Ca^{2+} -free buffer are bulkier and thus more compressible. The results demonstrate that the presence of Ca^{2+} makes the saccharide headgroups more compact and thus increases the intermolecular interaction in LPS Ra monolayers. In order to highlight the change in saccharide chain conformation, the influence of Ca^{2+} on the average LPS Ra structures perpendicular to the plane of the monolayers are deduced by measuring GIXOS on Ca^{2+} -free and Ca^{2+} -loaded buffers at a constant area per molecule, $A = 180 \text{ \AA}^2$ (Fig. 1). This condition was chosen to mimic the lateral density of LPS molecules in bacterial membranes.²

² The electron density profile is theoretically calculated to confirm the consistency with that deduced from the experiment: the number of water molecules is calculated by subtracting the volume occupied by all ions in each slab (thickness: 1.0 \AA).

2.2. Impact of Ca^{2+} on carbohydrate headgroups

Fig. 2A shows the GIXOS raw data of LPS Ra monolayers on Ca^{2+} -free (blue) and Ca^{2+} -loaded (red) buffers at $A = 180 \text{ \AA}^2$, together with the best fits corresponding to each data set (black solid lines). The GIXOS signal from a LPS Ra monolayer in the presence of Ca^{2+} is more intense than that on Ca^{2+} -free buffer, suggesting a higher electron density contrast. Furthermore, the fringe or shoulder-like feature on Ca^{2+} -loaded buffer appears at slightly higher q_z range, which implies that the presence of Ca^{2+} causes a decrease in total film thickness. For the fitting of the measured GIXOS curves, we use a two-slab model at the air/water interface: the first slab represents hydrocarbon chains and the second carbohydrate headgroups. Note that one slab is not sufficient to describe the experimental results. To exclude unphysical scenarios, we take some starting parameters for the first slab (hydrocarbon chains) by referring to the values reported at almost the same chain density [13]. In order to highlight the conformational change of carbohydrate headgroups, the parameters for the second slab are allowed to float during the fittings. The electron density and thickness of each slab, and the roughness of all the interfaces that correspond to the curves in Fig. 2A are summarized in Table 1.

Fig. 2B represents the electron density profiles normal to the membrane plane reconstructed from the fitting results. As presented in Table 1, the thickness of the hydrocarbon chains as well as the interface roughness between air and hydrocarbon chains is almost unchanged with or without Ca^{2+} . The difference in the chain/headgroups interface roughness between two buffers ($\sigma = 9.3$ and 6.6 \AA on Ca^{2+} -free and Ca^{2+} -loaded buffers, respectively) can be well explained by an increase of lateral cooperativity in the presence of Ca^{2+} , suggested by the global shapes of the pressure–area isotherms (Fig. 1). A more significant difference can be found in the conformation of carbohydrate headgroups. In the absence of Ca^{2+} (Fig. 2B blue curve), the carbohydrate chain is extended towards the bulk water. Here, the thickness and roughness at the headgroup/water interface are $d = 29.8 \text{ \AA}$ and $\sigma = 8.2 \text{ \AA}$, respectively. The total thickness of the LPS Ra monolayer in (i.e. the sum of two slabs) Ca^{2+} -free buffer is 38.79 \AA . This value agrees well with one half of the periodicity of LPS Ra multiple bilayers suspended in the same Ca^{2+} -free buffer (unpublished data), although this lamellar periodicity in dispersions should include the thickness of the water layer between neighboring bilayers. This can be partly attributed to the fact that neighboring membranes in dispersions are not

physically decoupled and maintain a finite distance, comparable to their surface roughness. On Ca^{2+} -loaded buffer, a decrease in the thickness of the carbohydrate headgroups can be seen ($d = 20.2 \text{ \AA}$), accompanied by a decrease in the roughness of the headgroup/water interface, $\sigma = 6.5 \text{ \AA}$. This can be attributed to a collapse of carbohydrate chains in the presence of Ca^{2+} – the corresponding electron density profile (red curve in Fig. 2B) shows an increase in the headgroup region in the vicinity of the air/water interface.

Fig. 3A shows the minimal model of LPS Ra. Since the GIXOS results (Fig. 2 and Table 1) suggest that the thickness, electron density, and the roughness at the air/chain interface are almost unchanged with and without Ca^{2+} at $A = 180 \text{ \AA}^2$, we model the hydrocarbon chain region ($z < 0$) as the portion of the large anchoring sphere of radius, R_{anchor} , with its center located at $z = z_0 < 0$. In Fig. 3B, we plot the calculated number-density distributions $\Phi(z)$ of Na^+ (blue), Ca^{2+} (red), and saccharides (green) in 1.0 \AA thick simulation slabs ($z = 0\text{--}40 \text{ \AA}$) for LPS Ra monolayers on Ca^{2+} -free (dashed lines) and Ca^{2+} -loaded (solid lines) buffers at $A = 180 \text{ \AA}^2$ [3]. There are six points to notice: (i) there is a peak in the LPS distribution in the inner core region irrespective of the presence/absence of Ca^{2+} ; (ii) the LPS peak height increases and is manifested at a lower z -value when Ca^{2+} is present; (iii) in the absence of Ca^{2+} , there is a Gaussian-like distribution of Na^+ in the vicinity of the six negatively charged sugars; (iv) in the presence of Ca^{2+} , most of Na^+ in the inner core region are replaced by Ca^{2+} within a few MC steps; (v) Cl^- is repelled from this region and is uniformly distributed at $z > 30 \text{ \AA}$ (data not shown); and (vi) there is a negative charge density around $z = 20 \text{ \AA}$ that shifts towards large z -values in the presence of Ca^{2+} , together with a positive charge density near $z = 5 \text{ \AA}$ which is increased in the presence of Ca^{2+} . Instantaneous conformations of carbohydrate headgroups (green) in Ca^{2+} -free and Ca^{2+} -loaded buffers obtained from computer simulation are presented in Fig. 3C and D, respectively. It can be seen that Ca^{2+} (red) condenses and forms salt bridges with negatively charged saccharides in the inner core region, which causes the collapse of carbohydrate headgroups towards the $z = 0$ plane. This is in excellent agreement with the electron density profiles reconstructed from the experiments (Fig. 2B).

2.3. Impact of protamine

Interactions of LPS Ra monolayers with CAPs in the presence and absence of Ca^{2+} are studied by

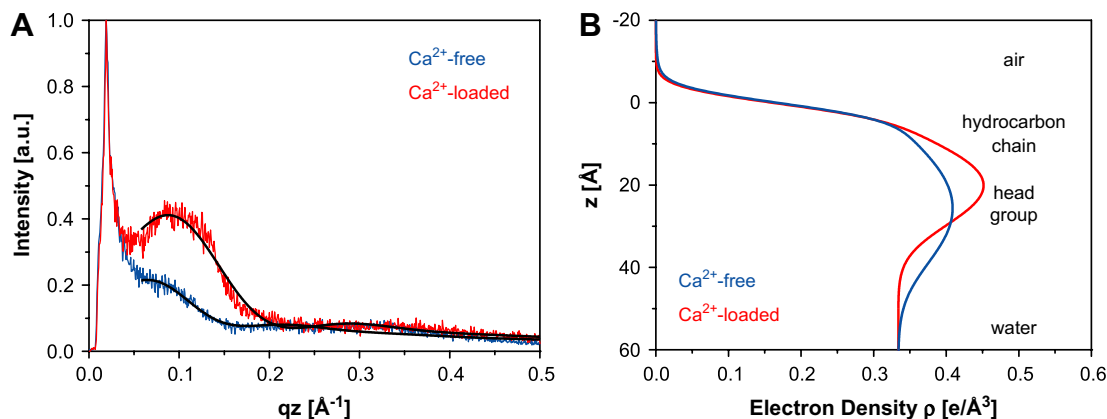


Fig. 2. A. GIXOS raw data from LPS Ra monolayers on Ca^{2+} -free (blue) and Ca^{2+} -loaded (red) buffers at $A = 180 \text{ \AA}^2$. The fitting curves (black) corresponding to the models are superimposed to the raw data. B. Electron density profiles along the z -axis of LPS Ra monolayers on Ca^{2+} -free (blue) and Ca^{2+} -loaded (red) buffer.

injecting herring protamine to the subphase at $A = 180 \text{ \AA}^2$. The final concentration of protamine is adjusted to be 1 mg ml^{-1} , which is comparable to the minimum inhibitory concentrations determined by *in vivo* experiments (1.25 mg ml^{-1}) [14]. Prior to the experiments with LPS Ra monolayers, surface pressures of both buffers in the presence of 1 mg ml^{-1} protamine remains zero. This confirms that the amount of protamine at the air/water interface (also called the surface excess) is negligibly small in the absence of LPS Ra monolayers, i.e. the surface activity of protamine itself plays no major role. In Fig. 4A, surface pressures of LPS Ra monolayers are plotted as a function of time on Ca^{2+} -free (blue) and Ca^{2+} -loaded (red) buffers. As indicated by an arrow, the time at which the protamine solution is injected is defined as $t = 0$. On Ca^{2+} -free buffer (blue), the surface pressure rapidly increases up to $\pi \sim 45 \text{ mN m}^{-1}$.³ Such a significant increase in the surface pressure ($\Delta\pi \sim 15 \text{ mN m}^{-1}$) cannot be explained by the adsorption of protamine to saccharide headgroup surfaces, but indicates that protamine goes deeper into the inner core region towards the air/water interface (Supporting information, Fig. 1) and disturbs the lateral cooperativity of LPS Ra molecules. The GIXOS curve measured at a new equilibrium ($\pi \sim 45 \text{ mN m}^{-1}$) cannot be interpreted with any slab model, indicating that the vertical layer-by-layer structure is destroyed (data not shown). In the presence of Ca^{2+} (red line), however, the surface

pressure remains constant at $\pi = 25 \text{ mN m}^{-1}$. This finding suggests that protamine does not reach to the air/water interface. The GIXOS curve and the reconstructed electron density profile show no detectable change before and after the protamine injection (see Supporting information, Fig. 2).

The results for the effect of Ca^{2+} upon the carbohydrate groups (Fig. 3B) suggest that an energy barrier is created against the diffusion of protamine molecules towards the hydrocarbon chain region. Fig. 4B shows number-density distributions in the presence of protamine molecules (Ptm, black), calculated for Ca^{2+} -loaded (solid lines) and Ca^{2+} -free (dashed lines) buffers. Here we considered a “high” protamine concentration, requiring that 5 protamine molecules occupied the simulation volume. Note that all protamines remain in the proximity of the monolayer

Table 1
Summary of GIXOS results

Layer	ρ ($\text{e}/\text{\AA}^3$)	d (\AA)	σ (\AA)
Ca^{2+} -free buffer			
Air	0	N/A	N/A
Hydrocarbon chain	0.30	9.0	3.2
Carbohydrate head	0.42	29.8	9.3
Water	0.33	N/A	8.2
Ca^{2+} -loaded buffer			
Air	0	N/A	N/A
Hydrocarbon chain	0.29	9.3	3.2
Carbohydrate head	0.47	20.2	6.6
Water	0.33	N/A	6.5

The structural parameters of each layer (electron density ρ , thickness d , and roughness σ) corresponding to the least square fits (Fig. 2A), which are also used to reconstruct the vertical electron density profiles (Fig. 2B).

³ Protamine solution is injected into the subphase from several different points outside of the compression barrier. Here, the characteristic time to reach equilibrium depends on the area and geometry of the sample, but the final surface pressure at equilibrium is unchanged.

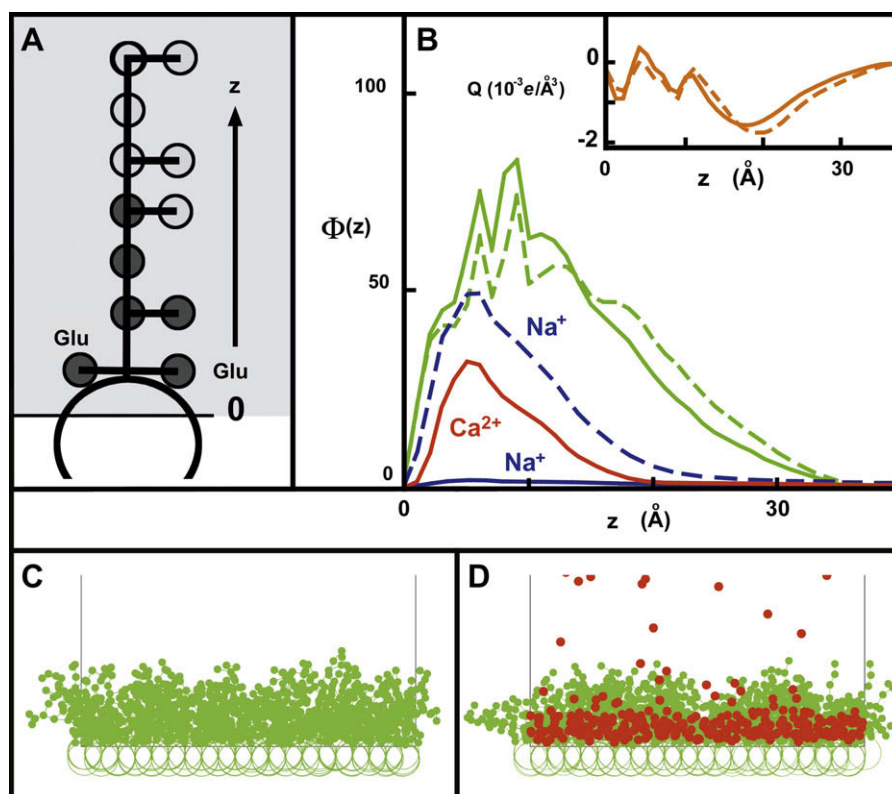


Fig. 3. A. Minimal structural model of LPS Ra used in MC simulations. $z=0$ is the boundary between the aqueous region ($z > 0$) and the hydrocarbon chain region ($z < 0$) represented by the portion of the large anchoring sphere of radius, R_{anchor} . Saccharides are represented by spheres of radius r_{sugar} connected by stretchable bonds of the following equilibrium lengths; $L_0 = 6.24 \pm 2.08$ Å for bonds between glucosamine (Glu) and anchors, and 5.2 ± 1.04 Å for bonds between saccharides in the core, as well as for their connecting bonds to anchors. Charged sugars (each -1 in units of $e = 1.6 \times 10^{-19}$ C) are dark spheres while uncharged sugars are light spheres. B. Number-density distributions without protamine, with (without) CaCl_2 at $A = 180$ Å². Solid (dashed) lines show core (green), Na^+ (blue), Ca^{2+} (red) and electric charge density distribution (insert, orange). C and D. Instantaneous conformations without (C) and with (D) CaCl_2 showing core (green) and Ca^{2+} (red).

during the simulations. As demonstrated for protamine-free systems in Ca^{2+} -loaded buffer (Fig. 3B), Na^+ (blue) in the core region is replaced by Ca^{2+} (red). Due to the formation of salt bridges via Ca^{2+} condensed in the inner core region, the saccharide chains collapse towards the air/water interface ($z=0$ plane), as indicated by GIXOS experiments (Fig. 2B) and simulation (Fig. 3B). The higher positive charge density near $z=5$ Å in the presence of Ca^{2+} compared to that in Ca^{2+} -free buffer, creates a higher energy barrier against penetration by protamine (Fig. 3B inset). This, together with the negative charge density minimum near $z=20$ Å, results in a shift of the protamine distribution towards a higher z -value (Fig. 4B). A typical instantaneous conformation (Fig. 4C) shows that only three protamine molecules (represented as black ball-chains) are partially immersed in the region enriched with Ca^{2+} (red). However, the number of

protamine molecules entering the Ca^{2+} -enriched region is too small to alter the electron density profile calculated from the scattering experiments. Note that the destruction of the layered structure does not permit us to create a reliable model in Ca^{2+} -free buffer, since the basic assumption (intactness of hydrocarbon chain layer) does not hold any longer. A recent report demonstrated that the presence of Ca^{2+} alters not only the saccharide chain conformation but also the mobility of hydrocarbon chains, which significantly influences the activity of LPSs [15]. Change in the entropic force due to changes in the conformations of the saccharide chains is also an aspect that we are in the process of considering. This aspect, together with a better model of the hydrocarbon chain region, is being developed to study both entropic repulsion and to better understand the penetration of CAPs into the hydrophobic region.

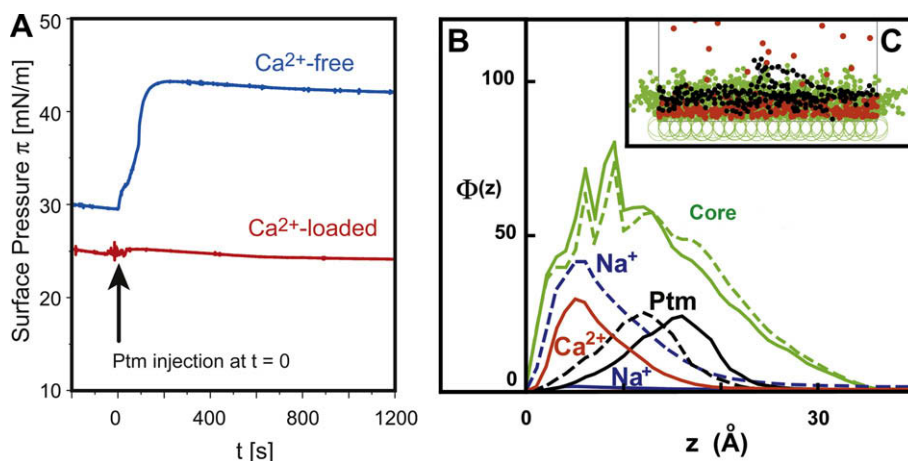


Fig. 4. Interactions of protamine and LPS Ra monolayers. A. Surface pressures of LPS Ra monolayers plotted as a function of time on Ca²⁺-free (blue) and Ca²⁺-loaded (red) buffers at $A = 180 \text{ \AA}^2$. Upon injection of protamine (Ptm) solution at $t = 0$ (the final concentration $\sim 1 \text{ mg ml}^{-1}$, comparable to the MIC), a significant increase in the surface pressure is observed on Ca²⁺-free buffer (blue), indicating the intrusion of the protamine into the LPS Ra monolayer. However, no change in the surface pressure can be observed in the presence of Ca²⁺. B. Number-density distributions for cases with (without) CaCl₂, solid (dashed) lines showing core (green), Na⁺ (blue), Ca²⁺ (red) and 5 protamine molecules (Ptm, black). C. Instantaneous conformation with CaCl₂ showing core (green), Ca²⁺ (red) and 5 protamine molecules (black).

3. Conclusions

By the complementary combination of a GIXOS and modeling with MC simulation, we successfully demonstrated for the first time the physical mechanisms of how bacteria survive against CAPs in the presence of Ca²⁺. The electron density profiles reconstructed from GIXOS signals imply the “collapse” of saccharide chains towards the air/water interface in the presence of Ca²⁺. The theoretical model demonstrates that the collapse of saccharide chains in Ca²⁺-loaded buffer is caused by the replacement of Na⁺ in the inner core region by Ca²⁺ and formation of Ca²⁺-ion bridges between negatively charged saccharide moieties. LPS Ra monolayers with Ca²⁺ ions form a barrier against protamine even near the MIC, showing no change in the surface pressure. In the presence of Ca²⁺, the electron density profile of the LPS Ra monolayer is unchanged by protamine. This is supported by the results of the theoretical model showing the creation of a charge density barrier. In contrast, a significant increase in the surface pressure ($\Delta\pi \sim 15 \text{ mN m}^{-1}$) compared to the Ca²⁺-loaded buffer indicates that protamine goes deeper into the inner core region towards the air/water interface. In fact, GIXOS signals cannot be interpreted by any slab model, indicating that the layered structure is destroyed even up to the hydrocarbon chain region. Further development of experimental settings, e.g. grazing-incidence X-ray fluorescence [16], would allow us for further details of ion distributions on biological surfaces.

4. Materials and methods

4.1. Sample preparation

LPS Ra was extracted from *S. enterica* (serovar Minnesota) rough strain, and the purified sample was lyophilized as reported [17]. MALDI-TOF mass spectrometry shows a sharp peak at 1797 Da, corresponding to the molecular weight of the lipid A portion with a hexa-acyl lipid anchor. To study the influence of Ca²⁺ ions, we used two types of subphases: (i) “Ca²⁺-free” buffer that consists of 5 mM HEPES and 100 mM NaCl, and (ii) “Ca²⁺-loaded” buffer that additionally contains 50 mM CaCl₂. Herring protamine (chloride salt) was purified by the method reported previously [18]. Pressure–area isotherms were recorded with a Langmuir film balance (Kibron Inc., Finland). After spreading the aqueous suspension of LPS Ra,⁴ the film was compressed at a constant speed of 1–10 Å² per molecule per minute.

4.2. Grazing-incidence X-ray scattering

GIXOS and GIXD measurements are conducted at ID10B beamline of the European Synchrotron Radiation Facility (ESRF, Grenoble, [Supporting information](#),

⁴ Since LPS Ra cannot easily be dissolved in organic solvents, an aqueous suspension of LPS Ra (2 mg ml^{-1}) is deposited on the subphase. Monolayers are stable upon compression and relaxation cycles.

Fig. 3). The LPS monolayer deposited on a homemade Langmuir film balance is kept in He atmosphere to minimize the radiation damage. The monochromatic beam ($\lambda = 1.547 \text{ \AA}$) illuminates the monolayer at an incident angle ($\alpha_i = 0.119^\circ$) slightly below the critical angle of the air/water interface. In the GIXOS measurements, the intensity of the scattered beam is collected with a position sensitive linear detector perpendicular to the monolayer surface at an azimuth angle near the incidence plane ($q_{\parallel} \sim 0.029 \text{ \AA}^{-1}$). In case in-plane momentum transfer is very small ($q_{\parallel} \sim 0$) and interface roughness is conformal, the measured diffuse intensity is connected to the corresponding reflectivity curve [11]:

$$I(q_z) \propto |T(k_{\text{out}})|^2 \frac{R(q_z)}{R_F(q_z)}. \quad (1)$$

Here, $I(q_z)$ denotes the intensity measured in a GIXOS experiment, $R(q_z)$ is the corresponding specular reflectivity as measured in a $\theta-2\theta$ scan, $R_F(q_z)$ denotes the specular reflectivity from a flat (ideal) surface and $T(k_{\text{out}})$ represent the characteristic Vineyard Function for the grazing-incidence configuration. The data are fitted using a self-developed routine to obtain a least square fit to each result. The calculations are based on the Master-Formula for specular reflectivity:

$$R(q_z) = R_F(q_z) \left| \frac{1}{\rho} \int \frac{d\rho(z)}{dz} \exp(iq_z z) dz \right|^2 \quad (2)$$

Note that the data points below $q_z = 0.06 \text{ \AA}^{-1}$ are not included in the fit, because the Master-Formula loses its validity for low q_z .

4.3. Modeling and computer simulation

4.3.1. Choice of the model

The air/water interface is the xy -plane with unit vectors \hat{x} , \hat{y} , and \hat{z} . On a scale of $\sim 2 \text{ \AA}$, the experimental resolution, the charge density is neither uniform nor static, and multivalent ions can form bridges between charged LPS moieties. These considerations render DLVO theory inadequate. The interactions that distinguish between the molecular components are hydrogen bonding and electrostatics. The simulation volume must be large enough to simulate $\geq 10^2$ LPS molecules, $\geq 10^3$ divalent cations and twice as many monovalent ions, and must sample conformational changes occurring on time-scales $> 10^{-3}$ s. Accordingly, we do not use atomic models, but create a “minimal model” [19] and use MC simulation

[20,21] with periodic boundary conditions along the x - and y -axes. At each MC step, we attempt to change the position of all moieties consistent with two requirements: no two moieties should overlap and no water-soluble moiety is permitted to enter the region $z < 0$.

4.3.2. Electrostatic interactions

The aqueous solution ($z > 0$) and the hydrocarbon chain region ($z < 0$) are represented as two dielectric continua with relative permittivities $\epsilon_w = 81$ and $\epsilon_{hc} = 5$, respectively [22,23], and we represent monovalent ion screening in the aqueous solution by linearized Poisson–Boltzmann theory [8,22,24,25]. We calculate the electric potential at $\vec{R} = x\hat{x} + y\hat{y} + z\hat{z}$ due to an electric charge Q at $\vec{R}_0 = x_0\hat{x} + y_0\hat{y} + z_0\hat{z}$ in the aqueous solution. Netz [19] derived expressions for the electrical potential at \vec{R} (Eqs. 14 and 15 in Ref. [19]). Since $\epsilon_{hp} \ll \epsilon_w$ giving $\eta = \epsilon_{hp}/\epsilon_w \approx 0.06$, the expression for the potential simplifies. Defining $\chi = (1-\eta)/(1+\eta)$ (Ref. [19], Eq. 20), the electrical potential at \vec{R} becomes,

$$V(Q, \vec{R}_0, \vec{R}) = (1/4\pi\epsilon_w\epsilon_0) \sum_j Q_{if}(|\vec{R}_j|), \quad (3)$$

$$f(|\vec{R}_j|) = e^{-\kappa|\vec{R}_j|}/|\vec{R}_j|$$

where the sum is over $j = 1-2$, $\vec{R}_1 = \vec{R} - \vec{R}_0$, $\vec{R}_2 = \vec{R} - \vec{R}_0 + 2z_0\hat{z}$, $Q_1 = Q$, and $Q_2 = \chi Q$, and κ^{-1} is the Debye screening length. The potential (Eq. 3) goes to two correct limiting values as $\epsilon_{hp} \rightarrow 0$ or as $\kappa \rightarrow 0$.

4.3.3. Definition of systems, simulation

The membrane plane of our simulation volume possesses dimensions $140 \times 122 \text{ \AA}^2$, enabling us to use 100 LPS molecules and the z dimension of this volume ranges from $0 \leq z \leq 200 \text{ \AA}$. Each saccharide group is represented by a sphere of radius $r_{\text{sugar}} = 1.5 \text{ \AA}$ (Fig. 3A), connected by stretchable bonds with equilibrium lengths L_0 [26,27]. We restrict the relative angle between the saccharide–saccharide bonds of these semi-flexible molecules to be $30 \pm 10^\circ$ [8]. Charged sugars possess charge -1 in units of $e = 1.6 \times 10^{-19} \text{ C}$ at their centers (Fig. 3A). Since our main focus is to study the effects of Ca^{2+} and protamine on saccharide chain conformation, the hydrocarbon chain region is represented by a portion of an anchoring sphere of radius, $R_{\text{anchor}} = 7.0 \text{ \AA}$ centered at $z_0 = -4.0 \text{ \AA}$. Molecules can move along z -axis by $\pm 1.5 \text{ \AA}$ from equilibrium. An anchoring sphere can rotate around its center but no moiety can move their centers into the region $z < 0$ [20,26,28].

Hydrated ions are represented by spheres of radius $r_1 = 1.8 \text{ \AA}$, with charges located at their centers. We choose $\kappa = 0.05 \text{ \AA}^{-1}$ (ionic strength $\sim 25 \text{ mM}$), and add sufficient monovalent ions so that, with $\kappa^2 = \kappa_1^1 + \kappa_2^2$ [29], we effectively have $\kappa = 0.10 \text{ \AA}^{-1}$ in the bulk. The “bulk” is specified to be the upper half of the simulation volume, $100 < z < 200 \text{ \AA}$, which is, accordingly, required to contain an average of 76 Na^+ and 76 Cl^- . Corresponding to the experimental conditions, we consider two buffers in the bulk: (i) no divalent spheres (Ca^{2+} -free buffer), and (ii) an average of 50.5 divalent spheres and an additional 101 Cl^- spheres in the bulk (Ca^{2+} -loaded buffer). The system is equilibrated to $T = 300 \text{ K}$ for $>10^6$ Monte Carlo steps, and the properties of the system are measured for a further 10^6 steps.

Acknowledgement

We thank ESRF (Grenoble) for the synchrotron beam times, and L. Wiegart and S. O’Flaherty for their experimental assistance. This work has been supported by the Deutsche Forschungsgemeinschaft, the Fonds der Chemischen Industrie, the Natural Sciences and Engineering Research Council (NSERC) of Canada, the Canadian Advanced Foods and Materials Network (AFMNet-NCE), and the U.S. National Science Foundation through grant DMR-0206681. R.G.O. is thankful to Alexander von Humboldt Foundation for the research fellowship and E.S. thanks the State Baden Württemberg for the Ph.D. fellowship.

Supporting information

Supplementary data associated with this article can be found in the online version, at [doi:10.1016/j.crci.2008.06.020](https://doi.org/10.1016/j.crci.2008.06.020).

References

- [1] R.E.W. Hancock, D.S. Chapple, *Antimicrob. Agents Chemother.* 43 (1999) 1317.
- [2] T.D. Brock, *Can. J. Microbiol.* 4 (1958) 65.
- [3] L.T. Hansen, J.W. Austin, T.A. Gill, *Int. J. Food Microbiol.* 66 (2001) 149.
- [4] N.M. Islam, T. Itakura, T. Motohiro, *Bull. Jpn. Soc. Sci. Fish.* 50 (1984) 1705.
- [5] L.P. Kotra, D. Golemi, N.A. Amro, G.Y. Liu, S. Mobashery, *J. Am. Chem. Soc.* 121 (1999) 8707.
- [6] R.D. Lins, T.P. Straatsma, *Biophys. J.* 81 (2001) 1037.
- [7] R.M. Shroll, T.P. Straatsma, *Biopolymers* 65 (2002) 395.
- [8] D.A. Pink, L.T. Hansen, T.A. Gill, B.E. Quinn, M.H. Jericho, T.J. Beveridge, *Langmuir* 19 (2003) 8852.
- [9] K. Brandenburg, J. Andrä, M. Müller, M.H.J. Koch, P. Garidel, *Carbohydr. Res.* 338 (2003) 2477.
- [10] B. Jiao, M. Freudenberg, C. Galanos, *Eur. J. Biochem.* 180 (1989) 515.
- [11] S. Mora, J. Daillant, D. Luzet, B. Struth, *Europhys. Lett.* 66 (2004) 694.
- [12] K. Kjaer, J. Als-Nielsen, C.A. Helm, L.A. Laxhuber, H. Möhwald, *Phys. Rev. Lett.* 58 (1987) 2224.
- [13] C.A. Helm, P. Tippmannkroyer, H. Möhwald, J. Als-Nielsen, K. Kjaer, *Biophys. J.* 60 (1991) 1457.
- [14] R. Potter, L. Truelstrup Hansen, T. Gill, *Int. J. Food Microbiol.* 103 (2005) 23.
- [15] P. Garidel, M. Rappolt, A.B. Schromm, J. Howe, K. Lohner, J. Andrä, M.H.J. Koch, K. Brandenburg, *Biochim. Biophys. Acta* 1715 (2005) 122.
- [16] N.N. Novikova, E.A. Yurieva, S.I. Zheludeva, M.V. Kovalchuk, N.D. Stepina, A.L. Tolstikhina, R.V. Gaynutdinov, D.V. Urusova, T.A. Matkovskaya, A.M. Rubtsov, O.D. Lopina, A.I. Erko, O.V. Konovalov, *J. Synchrotron Radiat.* 12 (2005) 511.
- [17] K. Brandenburg, U. Seydel, *Biochim. Biophys. Acta* 775 (1984) 225.
- [18] T.A. Gill, D.S. Singer, J.W. Thompson, *Process Biochem.* 41 (2006) 1875.
- [19] R.R. Netz, *Phys. Rev. E* 60 (1999) 3174.
- [20] P.Y. Lai, K. Binder, *J. Chem. Phys.* 97 (1992) 586.
- [21] K. Binder, *Monte Carlo Simulation in Statistical Physics: An Introduction*, Springer, Berlin, 1988.
- [22] J.N. Israelachvili, *Intermolecular and Surface Forces*, Academic Press Inc., London, 1991.
- [23] D.A. Pink, M. Belaya, V. Levadny, B. Quinn, *Langmuir* 13 (1997) 1701.
- [24] M. Deserno, C. Holm, S. May, *Macromolecules* 33 (2000) 199.
- [25] V. Vlady, *Annu. Rev. Phys. Chem.* 50 (1999) 145.
- [26] A. Chakrabarti, P. Nelson, R. Toral, *J. Chem. Phys.* 100 (1994) 748.
- [27] I. Carmesin, K. Kremer, *Macromolecules* 21 (1988) 2819.
- [28] M.J. Stevens, K. Kremer, *Phys. Rev. Lett.* 71 (1993) 2228.
- [29] D.A. Pink, C.B. Hanna, B.E. Quinn, V. Levadny, G.L. Ryan, L. Fillion, A.T. Paulson, *Food Res. Int.* 39 (2006) 1031.